Nanoscale hetero-structured Co−Co(OH)$_2$ composite/amorphous carbon core/shell bi-functional electrocatalysts electrochemically evolved from metastable hexagonal-phase cobalt for overall water splitting

Lu, Pai; Chen, Xuyuan

Department of Microsystems, University of South-Eastern Norway

This is an Accepted Manuscript of an article published by Elsevier in *Electrochimica Acta* on May 24, 2021, version of record: https://doi.org/10.1016/j.electacta.2021.138517

Lu, P., & Chen, X. (2021). Nanoscale hetero-structured Co−Co(OH)2 composite/amorphous carbon core/shell bi-functional electrocatalysts electrochemically evolved from metastable hexagonal-phase cobalt for overall water splitting. *Electrochimica Acta*, *386*, Article 138517. https://doi.org/https://doi.org/10.1016/j.electacta.2021.138517

Nanoscale Hetero-Structured Co–$Co(OH)_2$ Composite/Amorphous Carbon Core/Shell Bi-Functional Electrocatalysts Electrochemically Evolved from Metastable Hexagonal-Phase Cobalt for Overall Water Splitting

Pai Lu*, Xuyuan Chen*

Department of Microsystems, University of South-Eastern Norway, Campus Vestfold,

Raveien 215, 3184 Borre, Norway

*Corresponding author

E-mail: Pai.Lu@usn.no, Xuyuan.Chen@usn.no

Abstract

Bi-functional electrocatalysts suited to alkaline water splitting systems are highly pursued, towards the most realistic application enabled by simplified electrolyzer design and cost-effective operation. Herein, a novel nanocomposite Co–$Co(OH)_2$/C electrocatalyst with nanoscale hetero-structured metastable hexagonal-phase Co (H-Co) crystallites and $Co(OH)_2$ crystallites encapsulated by amorphous carbon shells is developed. We employ a mild thermal decomposition route coupled with in-situ carbon deposition performed at 400 °C to prepare H-Co/C core/shell structured precursor. In a following controllable electrochemical transformation at room temperature the partial conversion of the metastable H-Co to $Co(OH)_2$ leads to the mutual embedding of nanoscale crystalline H-Co and $Co(OH)_2$ confined in the amorphous carbon shells. Taking advantage of the nanowire array morphology, carbon coated core/shell structure, nanoscale size, and the synergistic H-Co and $Co(OH)_2$ bi-components, an outstanding bi-functional electrocatalytic performance for overall water splitting is attained with proved small overpotentials (93 mV for hydrogen evolution reaction, 264 mV for oxygen evolution reaction at 10 mA cm^{-2}).

Key words: Water splitting, Bi-functional electrocatalyst, Nanocomposite, Cobalt, Cobalt Hydroxide

1. Introduction

Water splitting to clean hydrogen energy source is a straightforward and promising route for the expected sustainable energy strategy [1–4]. While, the-state-of-art expensive noble metal involved electrode systems (e.g., Pt as the best hydrogen evolution reaction (HER) catalyst [5–7], Ir-, Ru-based catalysts with excellent activities in (oxygen evolution reaction) OER [8–10]) are imposing restrictions to the large-scale application of this technique. Regarding this challenge, tremendous efforts have been devoted to exploration of non-noble metal based electrocatalysts as cost-effective alternatives [11–14]. Among the extensively investigated cost-effective catalysts, transition metal compounds are placing at the research frontier by virtue of their earth-abundant characteristics, high catalytic activities, and especially the wide opportunities of transition metal compounds as bi-functional electrocatalysts for overall water splitting [15–18], which readily facilitate the electrolyzer design and benefit to mitigate the risk in mutual contamination of anode and cathode [19–21].

Metallic cobalt (Co) and Co-compound based bi-functional electrocatalysts are one of the most well-developed category for overall water splitting since they are suitable for more realistic alkaline water splitting yet with outstanding catalytic property [22–25]. The Co-based chalcogenide, boride electrodes have presented promising catalytic activities for both OER and HER. However, the involved complicated preparation process make such catalysts difficult to be applied at a large scale [26–28]. Cobalt phosphide has been confirmed to be the most active catalyst with low overpotentials when used as both HER and OER catalysts. Whereas, the intrinsic toxicity of most phosphor sources needed for synthesis substantially restricted the versatility of cobalt phosphide electrocatalysts [29–32]. From the perspective of macroscale application, metallic cobalt, cobalt oxide, or hydroxide bi-functional electrocatalysts obtained via facile processing yet evolved from inexpensive and safe starting materials are of practical significance [33–36]. Ultrafine Co-based nano-electrocatalysts with conductive carbon

protective layers are ideal paradigm catalysts due to their great catalytic activity and working stability, which have attracted tremendous research interests [37–40]. High temperature thermal decomposition of metal organic framework (MOF) precursors is an intensively studied route to carbon coated nano-Co. By thermal treatment of the typical ZIF-MOF at 900 °C, the prepared ultrafine Co nanoparticles encapsulated in carbon-nanotubes-grafted graphene sheets was reported to have superior HER performance (108 mV overpotential to achieve 10 mA cm^{-2} in 1 M KOH) [41]. However, in this study the application potential as bi-functional electrocatalyst for both HER and OER has not been discussed. Zhang et al. employed similar MOF transformation strategy to prepare Co nanoparticles encapsulated in B/N co-doped nanocarbon [42], which could effectively work as bi-functional catalyst for overall water splitting. As an OER catalyst, an overpotential of 302 mV is required to reach the current density of 10 mA cm^{-2}. An overpotential of 117 mV is required to drive the current density of 10 mA cm^{-2} when applied as HER catalyst. In this electrocatalyst preparation a high temperature thermal treatment process at 900 °C is also involved. The overpotentials for both HER and OER are still high, which thus led to a cell voltage of 1.68 V to achieve an electrolysis current density of 10 mA cm^{-2} for the prototype electrolyzer. Accordingly, to explore mild preparation routes to high performance Co/C nanocomposite electrocatalysts yet towards energy-saving production is of great significance.

Recently, transition metal/transition metal hydroxide nanocomposite has been explored as an outstanding bi-functional water splitting electrocatalyst both via theoretical prediction and experimental proof [43]. With respect to this new type of nanocomposite electrocatalyst, on one hand, the active defect sites across the metal-metal hydroxide interphase are benefiting to improve the OER performance. On the other hand, the lowered binding energy with atomic hydrogen enabled by the synergistic involvement of both metal component and metal hydroxide component leads to a superior HER catalytic performance. The pioneer study reported a unique

ultrathin two dimensional nanocomposite including co-existed Ni and $Ni(OH)_2$ crystallites at the nanoscale, and presented a very promising application potential of this composite as bi-functional electrocatalyst for alkaline overall water splitting [43]. While up to now, there are still scarce available preparation routes to this new type low cost bi-functional electrocatalyst. In this study, we first report a nanoscale hetero-structured Co–$Co(OH)_2$ bi-functional electrocatalyst via a novel preparation method based on electrochemical conversion of metastable H-Co to $Co(OH)_2$. The targeting electrocatalyst design merits in terms of ultrafine particle size (5–20 nm) for massive active sites, protective coating with conductive carbon layers for promised working stability, and synergistic bi-component (Co and $Co(OH)_2$) hetero-structure for enhanced catalytic property are all achieved in this paradigm electrocatalyst study. Moreover, the Co–$Co(OH)_2$/C electrocatalyst is prepared at a relatively mild thermal treatment condition (400 °C).

2. Experimental

2.1. Preparation of bi-functional electrocatalysts

Preparation of precatalysts: $Co(CO_3)_{0.5}(OH)\cdot 0.11H_2O$ nanowire arrays (NWAs) on carbon cloth (CC) substrates as the precursors were prepared by modification of a previous report [44]. In a typical synthesis, 4 mmol $Co(NO_3)_2$, 8 mmol NH_4F, and 20 mmol $CO(NH_2)_2$ were dissolved in 70 mL de-ionized (DI) water. Then the obtained solution was transferred into a 100 mL Teflon-lined stainless-steel autoclave. A piece of carbon cloth was immersed into the solution. Then the sealed autoclave was kept at 120 °C for 14 h. After cooling to room temperature naturally, the $Co(CO_3)_{0.5}(OH)\cdot 0.11H_2O$ NWA precursors were thoroughly cleaned by de-ionized water and ethanol for use. Subsequently, a mild thermal treatment coupled with chemical vapor deposition (CVD) process was deployed and performed in a furnace with quartz tube, to convert the obtained precursors to precatalysts. Specifically, $Co(CO_3)_{0.5}(OH)\cdot 0.11H_2O$

NWA samples were placed under vacuum, and when 5~10 mTorr was reached 500 sccm N_2 were introduced to maintain atmospheric pressure in the quartz tube. The furnace was heated up from room temperature to 400 °C at a rate of 2 °C min^{-1}, and then kept at 400 °C for 100 minutes. In the following step, 10 sccm C_2H_2 was added and held at 400 °C for 4 minutes. After natural cooling to room temperature under the protection of N_2, the samples were collected for use.

Preparation of evolved catalysts: The precatalysts were subjected to a continuous anodic polarization kept at a constant voltage (0.55 V vs Ag/AgCl) in a three-electrode system with 1 M KOH electrolyte for 3.5 hours at room temperature, in which the precatalysts grown on carbon cloth, Ag/AgCl reference electrode (saturated KCl), and Pt foil were respectively employed as the working electrode, reference electrode, and counter electrode.

2.2. Material characterization

Scanning electron microscopy (SEM, Hitachi S8230), transmission electron microscopy (TEM, FEI Titan G2 60-300) with energy dispersive X-ray (EDX) spectrum were used for characterization of the morphologies, element compositions, and crystallographic structures. X-ray powder diffraction (XRD) patterns were measured on a Bruker D8 diffractometer with a Cu Kα radiation.

2.3. Electrochemical performance characterization

The electrochemical measurements were performed both in three-electrode cells (electrocatalyst/CC working electrode, Ag/AgCl reference electrode (saturated KCl), Pt foil counter electrode) and 2-electrode full cells on a VMP3-Biologic electrochemical workstation with 1 M KOH electrolyte (saturated by N_2). The electrocatalyst samples grown on carbon cloth are directly used as the electrodes without any further treatment.

Three-electrode measurement: Linear sweep voltammetry (LSV) was performed at a scanning rate of 2 mV s^{-1}. All potentials in LSV were calibrated with respect to reversible

hydrogen electrode (RHE) via IR compensation based on following equation: P vs RHE = P vs Ag/AgCl + 0.059pH − IR. On the basis of the LSV, Tafel slope was derived. Electrochemical impedance spectroscopy (EIS) spectrum were performed over the frequency range from 100 mHz to 100 kHz with an AC perturbation of 10 mV at the potential of 0.55 V vs Ag/AgCl (or −1.15 V vs Ag/AgCl) for evaluating the impedance behavior of electrocatalysts involved in OER (or HER). Electrochemical active surface area (ECSA) evaluation was performed by cyclic voltammetry (CV) conducted at non-Faradaic region (0.1–0.2 V vs Ag/AgCl) to measure the apparent electrochemical double layer capacitance (Cdl).

Two-electrode full cell measurement: For overall water splitting measurement, the electrochemically evolved H-Co/$Co(OH)_2$/C was employed both as cathode and anode in the beaker-type prototype cell with 1 M KOH electrolyte. The electrocatalyst stability was evaluated by recording the potential vs time profile in a continuous electrolysis at a constant current density of 10 mA cm^{-2}.

3. Results and discussion

3.1. Structure characterization of H-Co/C precatalyst

Considering that metastable phase metal is more active [45,46], and accordingly could be chemically transformed to its oxidized derivatives with low energy barrier, herein we propose a strategy to achieve Co/$Co(OH)_2$ nanoscale hetero-structures via controllable electrochemical transformation of the metastable H-Co to $Co(OH)_2$. To prepare metastable nanoscale H-Co, a mild thermal treatment coupled with the following CVD of carbon (see Experimental) was employed to convert the $Co(CO_3)_{0.5}(OH)\cdot 0.11H_2O$ NWA precursor (see Fig. S1, Supporting Information) to H-Co/C nanocomposite, as shown in Fig. 1. Regarding H-Co is metastable and cannot exist stably at high temperature, the thermal treatment was controlled at a mild condition (400 °C). To keep the original NWA morphology of the precursors so that a large surface gain

and the favorable mass transfer can be achievable, a slow temperature ramping rate of 2 °C min^{-1} was adopted. The introduction of C_2H_2 at the end of the thermal decomposition of precursors is the essential step in preparation of metastable H-Co/C nanocomposite. The performed control experiment displayed that CoO was formed instead as the final product via exclusive thermal decomposition of the $Co(CO_3)_{0.5}(OH)\cdot 0.11H_2O$ precursors, without the coupled CVD process (see Fig. S2). Based on this experimental research, the coupled CVD indeed played two critical roles in facilitating the formation of H-Co/C nanocomposite: (1) As a commonly used CVD gas source, the thermal decomposition of C_2H_2 resulted in the coating of amorphous carbon layers onto the nanoparticles, (2) C_2H_2 was also employed as a reductant to transform the thermal decomposition derived CoO intermediate to H-Co. The low-magnification SEM characterization (Figs. 2a, b) proves that the NWA morphology was maintained after the thermal treatment. The nanowires with the diameter ranging from 100 nm to 200 nm were radially anchored onto the carbon fibers of carbon cloth. A typical high magnification SEM image (Fig. 2c) shows that the H-Co/C nanowire is constructed with interconnected tiny nanoparticles. TEM characterization (Figs. 2d, e) further demonstrates the detailed architecture, presenting the clear nanoparticles (size range of 5–20 nm) assembled nanowire morphology with abundant mesopores. The transformation from the smooth nanowires (see Fig. S1) to nanoparticles assembled nanowires (see Fig. 2c) is attributed to the significant weight loss from $Co(CO_3)_{0.5}(OH)\cdot 0.11H_2O$ precursor to CoO via the thermal decomposition and CoO intermediate to Co via the thermal reduction. The released gaseous products in this process led to the formation of plentiful mesopores. Consequently, the hierarchical macroporous–mesoporous structure endowed by NWA morphology and gapped interconnected nanoparticles presents an ideal electrocatalyst design for favorable mass transfer. The interconnected H-Co nanoparticles were encapsulated by thin amorphous carbon layers via the CVD of carbon, which is revealed by the high resolution TEM (HR-TEM) imaging (Figs.

2f, g). The H-Co/C core/shell structure can be further proved by the element mapping results (Fig. 2h). Fig. 2f clearly displays one typical highly crystalline H-Co particle encapsulated with ca. 2 nm amorphous carbon layers.

3.2. Study on partial conversion of H-Co to $Co(OH)_2$ via the electrochemical transformation

By taking the metastable property of H-Co, we employed an electrochemical conversion route to partially convert H-Co to $Co(OH)_2$ (see Experimental), thus a nanoscale hetero-structured H-Co/$Co(OH)_2$ composite encapsulated by amorphous carbon layers can be obtained (sketched in Fig. 1). As shown in Fig. 3a, the anode current increased substantially in the first 3.5 hours during the anodic polarization of the precatalyst H-Co/C at 0.55 V vs Ag/AgCl, which was mainly stemmed from the electron transfer contributed by the Co^0 to Co^{2+} redox involved in the transformation from H-Co to $Co(OH)_2$. After the partial conversion of H-Co within the first 3.5 hours, the anode current turned out to be stabilized up to 45 hours. The stable anode current is ascribed from the OER at a highly anodic potential. This stable current profile vs time can also be translated to a stable OER performance of the evolved H-Co/$Co(OH)_2$/C electrocatalyst. The conversion from H-Co to $Co(OH)_2$ was confirmed by XRD characterization (Fig. 3b). In the XRD pattern of H-Co/C precatalyst, all the XRD peaks are attributed to hexagonal phase Co (JCPDF no. 5–727) and graphitic carbon. In comparison, the newly appeared $Co(OH)_2$ diffraction peaks co-exist with the original H-Co peaks in the electrochemically evolved electrocatalyst. It should be noted that the inapparent weak diffraction signal of amorphous carbon is difficult to be identified compared with the much stronger diffraction signals of $Co(OH)_2$ crystallites. The irreversible evolution from H-Co to $Co(OH)_2$ can further be revealed by the electrochemical measurements. Figs. 3c, d present the CV measurements with the 1st to 3rd scanning cycles. Remarkable redox peaks appeared in the first 2 scanning cycles, while they disappeared since the 3rd scanning cycle. This clue indicates

that the irreversible redox reaction did happen during the initial anodic polarization, which corresponds to the transformation of H-Co to $Co(OH)_2$.

3.3. Structure characterization of the evolved H-Co/$Co(OH)_2$/C catalyst

The amorphous carbon layers of the H-Co/C precatalyst provided a confined space for crystal phase evolution from H-Co to $Co(OH)_2$, which assisted to restrain the formation of bigger crystallites and accordingly facilitate the mutual embedding of H-Co nanocrystallites and $Co(OH)_2$ nanocrystallites to form the nanoscale hetero-structures. SEM characterization (Figs. 4a–c) presents that the nanoparticle size and shape, as well as the assembled NWA hierarchical architecture were maintained unchanged via the crystal phase evolution. The mesoporous structure of the evolved H-Co/$Co(OH)_2$/C can be revealed by a low-magnification TEM image (Fig. 4j). The selected area element mapping of cobalt and carbon as shown in Figs. 4k, l confirms the inheritance of the original core/shell structure with about the same size range and shape. We further employed the HR-TEM characterization to perform the phase identification. Different crystalline areas can be detected in the electrochemically evolved catalyst (Fig. 4d). Figs. 4e, f display the highlighted crystal lattices attributed to (002) facets of H-Co. While, the (102) crystal lattices of $Co(OH)_2$ are shown in Figs. 4g, h. Additionally, the crystal defects (see Fig. 4i) was also observed to be located adjacent to the interphase of H-Co and $Co(OH)_2$, which could be possibly generated during the in-situ crystal phase transformation from H-Co to $Co(OH)_2$.

3.4. Catalytic performance comparison of H-Co/C and H-Co/$Co(OH)_2$/C catalysts

To demonstrate the performance superiority of the electrochemically evolved H-Co/$Co(OH)_2$/C catalyst compared with the H-Co/C precatalyst in bi-functional water splitting, we first respectively compared their OER and HER catalytic performance. The LSV measurements presented in Fig. 5a show that the overpotential at 10 mA cm^{-2} for OER (OER-η_{10mA}) of H-Co/$Co(OH)_2$/C is 264 mV, which is smaller than that of H-Co/C (295 mV). Also,

the measurement of HER overpotential at 10 mA cm^{-2} for H-Co/$Co(OH)_2$/C presented a significant decrease compared with the precatalyst H-Co/C nanocomposite (see Fig. 5b), showing 93 mV vs 160 mV. Fig. 5c displays that when the working electrodes were kept at −1.15 V vs Ag/AgCl, both the precatalyst and the evolved catalyst electrodes are capable of outputting steady cathode current, indicative of their steady working stability in alkaline environment as HER electrocatalysts. The achieved electrochemical stability is believed to be assisted by the conformal coating of amorphous carbon layers onto the Co-based active materials. This has been widely confirmed to be an effective design for stable electrocatalysts [47]. In comparison, the cathode current of H-Co/$Co(OH)_2$/C based electrode was stabilized at around 17 mA cm^{-2}, which is much higher than that of H-Co/C based cathode. All the aforementioned electrochemical measurement results prove the much better bi-functional catalytic activity of the electrochemically evolved catalyst compared with the precatalyst, towards overall water splitting. To gain more insights into the origin of the superior catalytic performance of H-Co/$Co(OH)_2$/C, the ECSA evaluation was performed based on calculating the double-layer capacitance (Cdl) (in proportion to ECSA) within a non-Faradic reaction region (0.1–0.2 V vs Ag/AgCl) in CV (Fig. S3) [41]. The voltammetry current as a function of the scanning rate, in connection with the calculated Cdl are displayed in Fig. 5d. Very high Cdl values are both achieved by H-Co/$Co(OH)_2$/C (379 mF cm^{-2}) and H-Co/C (260 mF cm^{-2}), which are contributed by the highly macro-/meso-porous structure. The higher ECSA of H-Co/$Co(OH)_2$/C relative to H-Co/C is also revealed. This rationally can be translated into that the electrochemically active surface areas for catalysis are much more available in H-Co/$Co(OH)_2$/C. The improved ECSA most probably is derived from the crystal defects generated during the evolution from H-Co to $Co(OH)_2$, which can contribute positively to both enhanced HER and OER performance. The defects sites in the evolved electrocatalyst have been observed in the TEM identification (Fig. 4i). Inferred from the electrochemical

measurement, the HER overpotential is more significantly diminished as shown in Fig. 5b. Apart from the contribution from ECSA improvement, the lowered binding energy with atomic hydrogen enabled by creating nanoscale hetero-structure with synergistic bi-component of H-Co and $Co(OH)_2$ is the other benefit, as that has been confirmed in $Ni/Ni(OH)_2$ nanocomposite electrocatalyst [43]. Such efficient interface engineering of nanoscale electrocatalysts has been regarded as an efficient strategy to improve the electrochemical water splitting performance [48–50]. Nyquist plots of H-$Co/Co(OH)_2$/C and H-Co/C electrocatalysts when worked for OER and HER in the EIS measurements are respectively displayed in Fig. 5e and Fig. 5f. The smaller semicircle diameter representing the smaller charge transfer resistance of H-$Co/Co(OH)_2$/C is also in good agreement with its greater electrocatalytic performance in comparison with H-Co/C when employed as both OER and HER electrocatalysts.

3.5. Water splitting performance of H-Co/Co(OH)$_2$/C compared with state-of-the-art catalysts

Fig. 6 shows the systematic performance study of H-$Co/Co(OH)_2$/C nanocomposite electrocatalyst. From the LSV measurement shown in Fig. 6a and Fig. 6c, the Tafel slopes for OER and HER can be derived (Figs. 6b, d). The electrocatalytic performance can be summarized to be: (1) As OER catalyst, OER-η_{10mA} is 264 mV, with a Tafel slope of 78 mV dec^{-1}, (2) As HER catalyst, HER-η_{10mA} is 93 mV, with a Tafel slope of 121 mV dec^{-1}. A prototype full cell electrolysis with H-$Co/Co(OH)_2$/C as both the OER catalyst and HER catalyst is built to demonstrate its bi-functional catalytic property (Fig. 6e). The inset photograph shows that the hydrogen and oxygen gas bubbles can be respectively evolved from the cathode and anode. To reach a water splitting current density at 10 mA cm^{-2}, a cell voltage of around 1.62 V is required in 1 M KOH electrolyte. Further, the long-term running stability was demonstrated with a very stable voltage profile as a function of time up to 19 hours. After the full cell water splitting, the nanowire array morphology of both the HER and OER catalysts was intactly maintained (details please see Fig. S4). Table 1 lists the current state-of-the-art

performance of Co-, CoO_x-, $Co(OH)_2$-based bi-functional water splitting catalysts, monofunctional HER catalysts, and monofunctional OER catalysts. The H-Co/$Co(OH)_2$/C electrocatalyst is confirmed to have the lowest overpotentials both for HER and OER among the bi-functional catalysts [34, 38, 42, 51–52]. Even compared with the monofunctional HER catalysts and OER catalysts [41, 53–54], our developed H-Co/$Co(OH)_2$/C electrocatalyst is also among the best performance.

4. Conclusions

In summary, we develop a new strategy to prepare high performance H-Co/$Co(OH)_2$/C nanocomposite bi-functional electrocatalyst for alkaline water splitting, based on partial electrochemical transformation of metastable phase H-Co to $Co(OH)_2$. The core/shell H-Co/C precatalyst with ultrafine H-Co nanoparticles encapsulated in amorphous carbon layers facilitates the confined in-situ crystal phase evolution to derive nanoscale hetero-structured H-Co/$Co(OH)_2$ with enhanced catalytic property. We combine four design merits in this novel H-Co/$Co(OH)_2$/C nanocomposite electrocatalyst: (1) ultrafine catalyst size (5–20 nm) enabling massive catalytic active sites, (2) macro-/meso-porous structure enabling improved mass transfer, (3) conductive carbon layer protection enabling promised working stability and great electron transfer, (4) nanoscale metal/metal hydroxide hetero-structure with synergistic bi-component and electrocatalytically active defect sites enabling enhanced HER and OER catalytic property. The proposed strategy based on controllable partial transformation of metastable metal to its oxidized derivative herein is expected to be extended to derive many other nanoscale hetero-structured electrocatalysts.

Credit Author Statement

Pai Lu: Conceptualization, experiments, and manuscript preparation

Xuyuan Chen: Project supervision, and manuscript preparation

Declaration of Competing Interests

The authors declare that they have no known competing financial interests or personal relationships that could have appeared to influence the work reported in this paper.

Acknowledgment

We acknowledge Dr. Kalliopi Bazioti and Prof. Øystein Prytz (Department of Physics, University of Oslo) for TEM characterization.

This work was supported by the strategic research plan "Energy and Climate Challenge" of University of South-Eastern Norway [2700078]; the Research Council of Norway through the Norwegian Center for Transmission Electron Microscopy, NORTEM [197405/F50].

References

[1] J. Greeley, T.F. Jaramillo, J. Bonde, I.B. Chorkendorff, J.K. Norskov, Computational high-throughput screening of electrocatalytic materials for hydrogen evolution, Nat. Mater. 5 (2006) 909–913.

[2] A. Munir, T. ul Haq, M. Saleem, A. Qurashi, S.Z. Hussain, F. Sher, A. Ul-Hamid, A. Jilani, I. Hussain, Controlled engineering of nickel carbide induced N-enriched carbon nanotubes for hydrogen and oxygen evolution reactions in wide pH range, Electrochim. Acta 341 (2020) 136032.

[3] M.F. Wang, S.S. Liu, T. Qian, J. Liu, J.Q. Zhou, H.Q. Ji, J. Xiong, J. Zhong, C. Yan, Over 56.55% Faradaic efficiency of ambient ammonia synthesis enabled by positively shifting the reaction potential, Nat. Commun. 10 (2019) 341.

[4] R.F. Service, New electrolyzer splits water on the cheap, Science 367 (2020) 1181–1181.

[5] Z. Li, R.X. Ge, J.W. Su, L. Chen, Recent progress in low Pt content electrocatalysts for hydrogen evolution reaction, Adv. Mater. Interfaces 7 (2020) 2000396.

[6] Q. Dang, Y.Y. Sun, X. Wang, W.X. Zhu, Y. Chen, F. Liao, H. Huang, M.W. Shao, Carbon dots-Pt modified polyaniline nanosheet grown on carbon cloth as stable and high-efficient electrocatalyst for hydrogen evolution in pH-universal electrolyte, Appl. Catal. B Environ. 257 (2019) 117905.

[7] Q.Q. Zhang, J.Q. Guan, Atomically dispersed catalysts for hydrogen/oxygen evolution reactions and overall water splitting, J. Power Sources 471 (2020) 228446.

[8] A. Lim, J. Kim, H.J. Lee, H.J. Kim, S.J. Yoo, J.H. Jang, H.Y. Park, Y.E. Sung, H.S. Park, Low-loading IrO_2 supported on Pt for catalysis of PEM water electrolysis and regenerative fuel cells, Appl. Catal. B Environ. 272 (2020) 118955.

[9] J.Z.Y. Seow, T.D. Nguyen, Electrochemically assisted synthesis of ultra-small Ru@IrO_x core-shell nanoparticles for water splitting electro-catalysis, Electrochim. Acta 341 (2020) 136058.

[10] E. Antolini, Iridium as catalyst and cocatalyst for oxygen evolution/reduction in acidic polymer electrolyte membrane electrolyzers and fuel cells, ACS Catal. 4 (2014) 1426–1440.

[11] N. Kim, D. Lim, Y. Choi, S.E. Shim, S.H. Baeck, Hexagonal beta-$Ni(OH)_2$ nanoplates with oxygen vacancies as efficient catalysts for the oxygen evolution reaction, Electrochim. Acta 324 (2019) 134868.

[12] J. Yang, A.R. Mohmad, Y. Wang, R. Fullon, X.J. Song, F. Zhao, I. Bozkurt, M. Augustin, E.J.G. Santos, H.S. Shin, W.J. Zhang, D. Voiry, H.Y. Jeong, M. Chhowalla, Ultrahigh-current-density niobium disulfide catalysts for hydrogen evolution, Nat. Mater. 18 (2019) 1309–1314.

[13] J. Kibsgaard, I. Chorkendorff, Considerations for the scaling-up of water splitting catalysts, Nat. Energy 4 (2019) 430–433.

[14] B.H.R. Suryanto, Y. Wang, R.K. Hocking, W. Adamson, C. Zhao, Overall electrochemical splitting of water at the heterogeneous interface of nickel and iron oxide, Nat. Commun. 10 (2019) 5599.

[15] L. Hui, Y.R. Xue, B.L. Huang, H.D. Yu, C. Zhang, D.Y. Zhang, D.Z. Jia, Y.J. Zhao, Y.J. Li, H.B. Liu, Y.L. Li, Overall electrochemical splitting of water at the heterogeneous interface of nickel and iron oxide, Nat. Commun. 9 (2018) 5309.

[16] S. Sultan, M. Ha, D.Y. Kim, J.N. Tiwari, C.W. Myung, A. Meena, T.J. Shin, K.H. Chae, K.S. Kim, Superb water splitting activity of the electrocatalyst $Fe_3Co(PO_4)_4$ designed with computation aid, Nat. Commun. 10 (2019) 5195.

[17] A. Muthurasu, G.P. Ojha, M. Lee, H.Y. Kim, Zeolitic imidazolate framework derived Co_3S_4 hybridized MoS_2-Ni_3S_2 heterointerface for electrochemical overall water splitting reactions, Electrochim. Acta 334 (2020) 135537.

[18] V.H. Hoa, D.T. Tran, H.T. Le, N.H. Kim, J.H. Lee, Hierarchically porous nickel cobalt phosphide nanoneedle arrays loaded micro-carbon spheres as an advanced electrocatalyst for overall water splitting application, Appl. Catal. B Environ. 253 (2019) 235–245.

[19] P.W. Menezes, A. Indra, I. Zaharieva, C. Walter, S. Loos, S. Hoffmann, R. Schlogl, H. Dau, M. Driess, Helical cobalt borophosphates to master durable overall water-splitting, Energy Environ. Sci. 12 (2019) 988–999.

[20] Y.H. Tang, Q. Liu, L. Dong, H.B. Wu, X.Y. Yu, Activating the hydrogen evolution and overall water splitting performance of NiFe LDH by cation doping and plasma reduction, Appl. Catal. B Environ. 266 (2020) 118627.

[21] R. Khan, M.T. Mehran, S.R. Naqvi, A.H. Khoja, K. Mahmood, F. Shahzad, S. Hussain, Role of perovskites as a bi-functional catalyst for electrochemical water splitting: A review, Int. J. Energy Res. 2020, in press, DOI: 10.1002/er.5635.

[22] J.H. Wang, W. Cui, Q. Liu, Z.C. Xing, A.M. Asiri, X.P. Sun, Recent progress in cobalt-based heterogeneous catalysts for electrochemical water splitting, Adv. Mater. 28 (2016) 215–230.

[23] W. Adamson, X. Bo, Y.B. Li, B.H.R. Suryanto, X.J. Chen, C. Zhao, Co-Fe binary metal oxide electrocatalyst with synergistic interface structures for efficient overall water splitting, Catal. Today 351 (2020) 44–49.

[24] P.W. Menezes, C. Panda, C. Walter, M. Schwarze, M. Driess, A cobalt-based amorphous bifunctional electrocatalysts for water-splitting evolved from a single-source Lazulite cobalt phosphate, Adv. Funct. Mater. 29 (2019) 1808632.

[25] Y.L. Liu, X.H. Luo, C.L. Zhou, S. Du, D.S. Zhen, B. Chen, J. Li, Q. Wu, Y. Iru, D.C. Chen, A modulated electronic state strategy designed to integrate active HER and OER components as hybrid heterostructures for efficient overall water splitting, Appl. Catal. B Environ. 260 (2020) 118197.

[26] L. Nisar, M. Sadaqat, A. Hassan, N.U.A. Babar, A. Shah, M. Najam-Ul-Haq, M.N. Ashiq, M.F. Ehsan, K.S. Joya, Ultrathin CoTe nanoflakes electrode demonstrating low overpotential for overall water splitting, Fuel 280 (2020) 118666.

[27] J. Masud, A.T. Swesi, W.P.R. Liyanage, M. Nath, Cobalt selenide nanostructures: An efficient bifunctional catalyst with high current density at low coverage, ACS Appl. Mater. Interfaces 8 (2016) 17292–17302.

[28] J. Masa, P. Weide, D. Peeters, I. Sinev, W. Xia, Z.Y. Sun, C. Somsen, M. Muhler, W. Schuhmann, Amorphous cobalt boride (Co_2B) as a highly efficient nonprecious catalyst

for electrochemical water splitting: Oxygen and hydrogen evolution, Adv. Energy Mater. 6 (2016) 1502313.

[29] B. Kim, T. Kim, K. Lee, J.H. Li, Recent advances in transition metal phosphide electrocatalysts for water splitting under neutral pH conditions, ChemElectroChem 7 (2020) 3578–3589.

[30] J. Joo, T. Kim, J. Lee, S.I. Choi, K. Lee, Morphology-controlled metal sulfides and phosphides for electrochemical water splitting, Adv. Mater. 31 (2019) 1806682.

[31] R. Boppella, J. Tan, W. Yang, J. Moon, Homologous CoP/NiCoP heterostructure on N-doped carbon for highly efficient and pH-universal hydrogen evolution electrocatalysis, Adv. Funct. Mater. 29 (2019) 1807976.

[32] Y.J. Lu, W.Q. Hou, D.X. Yang, Y.F. Chen, CoP nanosheets in-situ grown on N-doped graphene as an efficient and stable bifunctional electrocatalyst for hydrogen and oxygen evolution reactions, Electrochim. Acta 307 (2019) 543–552.

[33] Y.P. Zhu, T.Y. Ma, M. Jaroniec, S.Z. Qiao, Self-templating synthesis of hollow Co_3O_4 microtube arrays for highly efficient water electrolysis, Angew. Chem. Int. 56 (2017) 1324–1328.

[34] P. Guo, J. Wu, X.B. Li, J. Luo, W.M. Lau, H. Liu, X.L. Sun, L.M. Liu, A highly stable bifunctional catalyst based on 3D $Co(OH)_2$@NCNTs@NF towards overall water-splitting, Nano Energy 47 (2018) 96–104.

[35] M. Xu, L. Huang, Y.X. Fang, L. Han, Y. Yu, S.J. Dong, The unified ordered mesoporous carbons supported Co-based electrocatalysts for full water splitting, Electrochim. Acta 261 (2018) 412–420.

[36] P.W. Du, R. Eisenberg, Catalysts made of earth-abundant elements (Co, Ni, Fe) for water splitting: Recent progress and future challenges, Energy Environ. Sci. 5 (2012) 6012–6021.

[37] M. Yang, Y.Y. Yang, K.Z. Wang, S.W. Li, F. Feng, K. Lan, P.B. Jiang, X.K. Huang, H.L. Yang, R. Li, Facile synthesis of CoSe nanoparticles encapsulated in N-doped carbon nanotubes-grafted N-doped carbon nanosheets for water splitting, Electrochim. Acta 337 (2020) 135685.

[38] H.Y. Jin, J. Wang, D.F. Su, Z.Z. Wei, Z.F. Pang, Y. Wang, In situ cobalt–cobalt oxide/N-doped carbon hybrids as superior bifunctional electrocatalysts for hydrogen and oxygen evolution, J. Am. Chem. Soc. 137 (2015) 2688–2694.

[39] Q.R. Liang, H.H. Jin, Z. Wang, Y.L. Xiong, S. Yuan, X.C. Zeng, D.P. He, S.C. Mu, Metal-organic frameworks derived reverse-encapsulation Co-NC@Mo_2C complex for efficient overall water splitting, Nano Energy 57 (2019) 746–752.

[40] C. Huang, D.H. Wu, P. Qin, K. Ding, C.R. Pi, Q.D. Ruan, H. Song, B. Gao, H.Y. Chen, P.K. Chu, Ultrafine Co nanodots embedded in N-doped carbon nanotubes grafted on hexagonal VN for highly efficient overall water splitting, Nano Energy 73 (2020) 104788.

[41] Z.L. Chen, R.B. Wu, Y. Liu, Y. Ha, Y.H. Guo, D.L. Sun, M. Liu, F. Fang, Ultrafine Co nanoparticles encapsulated in carbon-nanotubes-grafted graphene sheets as advanced electrocatalysts for the hydrogen evolution reaction, Adv. Mater. 30 (2018) 1802011.

[42] M.R. Liu, Q.L. Hong, Q.H. Li, Y.H. Du, H.X. Zhang, S.M. Chen, T.H. Zhou, J. Zhang, Cobalt boron imidazolate framework derived cobalt nanoparticles encapsulated in B/N codoped nanocarbon as efficient bifunctional electrocatalysts for overall water splitting, Adv. Funct. Mater. 28 (2018) 1801136.

[43] L. Dai, Z.N. Chen, L.X. Li, P.Q. Yin, Z.Q. Liu, H. Zhang, Ultrathin Ni(0)-embedded $Ni(OH)_2$ heterostructured nanosheets with enhanced electrochemical overall water splitting, Adv. Mater. 32 (2020) 1906915.

[44] Y. Wang, Y.M. Ni, B. Liu, S.X. Shang, S. Yang, M.H. Cao, C.W. Hu, Vertically oriented CoO@FeOOH nanowire arrays anchored on carbon cloth as a highly efficient electrode for oxygen evolution reaction, Electrochim. Acta 257 (2017) 356–363.

[45] X. Liu, M.M. Steiner, R. Sooryakumar, Exchange stiffness, magnetization, and spin waves in cubic and hexagonal phases of cobalt, Phys. Rev. B 53 (1996) 12166–12172.

[46] X.Y. Tan, S.Z. Geng, Y.J. Ji, Q. Shao, T. Zhu, P.T. Wang, Y.Y. Li, X.Q. Huang, Closest packing polymorphism interfaced metastable transition metal for efficient hydrogen evolution, Adv. Mater. 2020, in press, DOI: 10.1002/adma.202002857.

[47] D.T. Tran, T. Kshetri, D.C. Nguyen, J. Gautam, V.H. Hoa, H.T. Le, N.H. Kim, J.H. Lee, Emerging core-shell nanostructured catalysts of transition metal encapsulated by two-dimensional carbon materials for electrochemical applications, Nano Today 22 (2018) 100–131.

[48] H. Xu, H.Y. Shang, C. Wang, Y.K. Du, Surface and interface engineering of noble-metal-free electrocatalysts for efficient overall water splitting, Coord. Chem. Rev. 418 (2020) 213374.

[49] A.P. O'Mullane, Creating active interfaces as a strategy to improve electrochemical water splitting reactions, J. Phys. Energy 2 (2020) 041001.

[50] B. Singh, A. Indra, Surface and interface engineering in transition metalebased catalysts for electrochemical water oxidation, Mater. Today Chem. 16 (2020) 100239.

[51] Z.K. Yang, C.M. Zhao, Y.T. Qu, H. Zhou, F.Y. Zhou, J. Wang, Y. Wu, Y.D. Li, Trifunctional self-supporting cobalt-embedded carbon nanotube films for ORR, OER, and HER triggered by solid diffusion from bulk metal, Adv. Mater. 31 (2019) 1808043.

[52] X.X. Yu, Z.Y. Yu, X.L. Zhang, P. Li, B. Sun, X.C. Gao, K. Yan, H. Liu, Y. Duan, M.R. Gao, G.X. Wang, S.H. Yu, Highly disordered cobalt oxide nanostructure induced by sulfur incorporation for efficient overall water splitting, Nano Energy 71 (2020) 104652.

[53] J.X. Feng, L.X. Ding, S.H. Ye, X.J. He, H. Xu, Y.X. Tong, G.R. Li, $Co(OH)_2$@PANI hybrid nanosheets with 3D networks as high-performance electrocatalysts for hydrogen evolution reaction, Adv. Mater. 27 (2015) 7051−7057.

[54] M. Kim, B. Lee, H. Ju, S.W. Lee, J. Kim, Reducing the barrier energy of self-reconstruction for anchored cobalt nanoparticles as highly active oxygen evolution electrocatalyst, Adv. Mater. 31 (2019) 1901977.

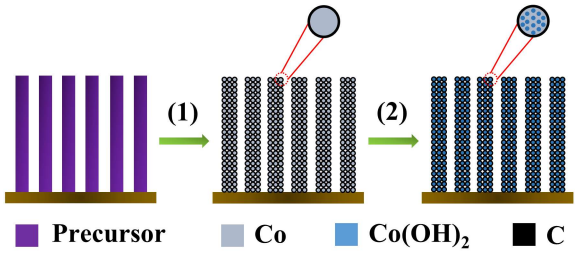

Fig. 1. Sketch of the transformation from $Co(CO_3)_{0.5}(OH)\cdot 0.11H_2O$ precursor NWAs to H-Co/C intermediate and the electrochemically evolved H-Co/$Co(OH)_2$/C catalyst via the sequential processing: (1) thermal decomposition coupled with in-situ carbon deposition, (2) electrochemical transformation.

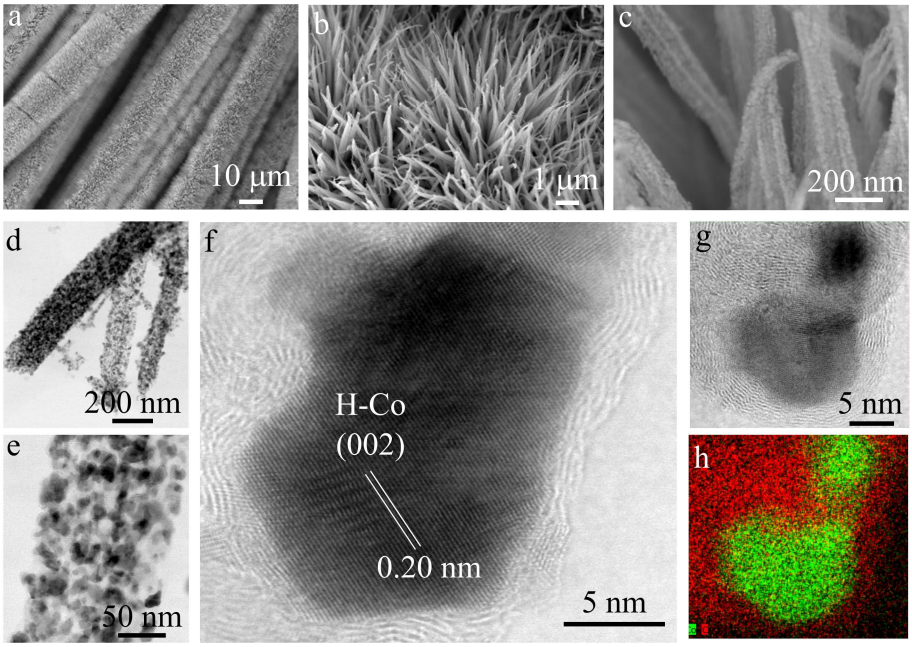

Fig. 2. a–c) SEM images of the H-Co/C precatalyst at different magnifications. d, e) Low magnification TEM images and f) HRTEM image of the H-Co/C precatalyst. g, h) Selected area EDX element mapping results to reveal the H-Co/C core/shell structure (Green color: Co, Red color: Carbon).

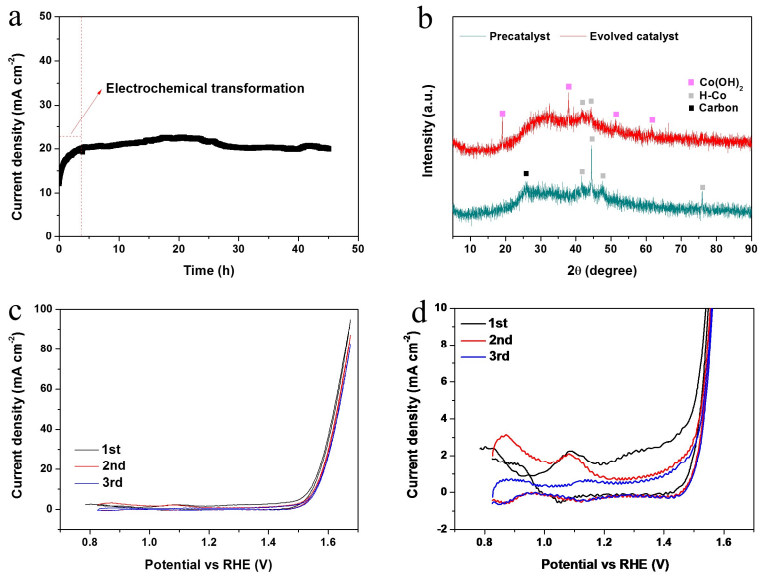

Fig. 3. a) Electrochemical polarization of the H-Co/C precatalyst at 0.55 V vs Ag/AgCl. b) XRD characterization of the H-Co/C precatalyst and the evolved catalyst H-Co/$Co(OH)_2$/C (H-Co (JCPDF no. 5–727), $Co(OH)_2$ (JCPDF no. 30–443)). c, d) CV measurement of the H-Co/C precatalyst at the first three cycles with a scanning rate of 1 mV s^{-1}.

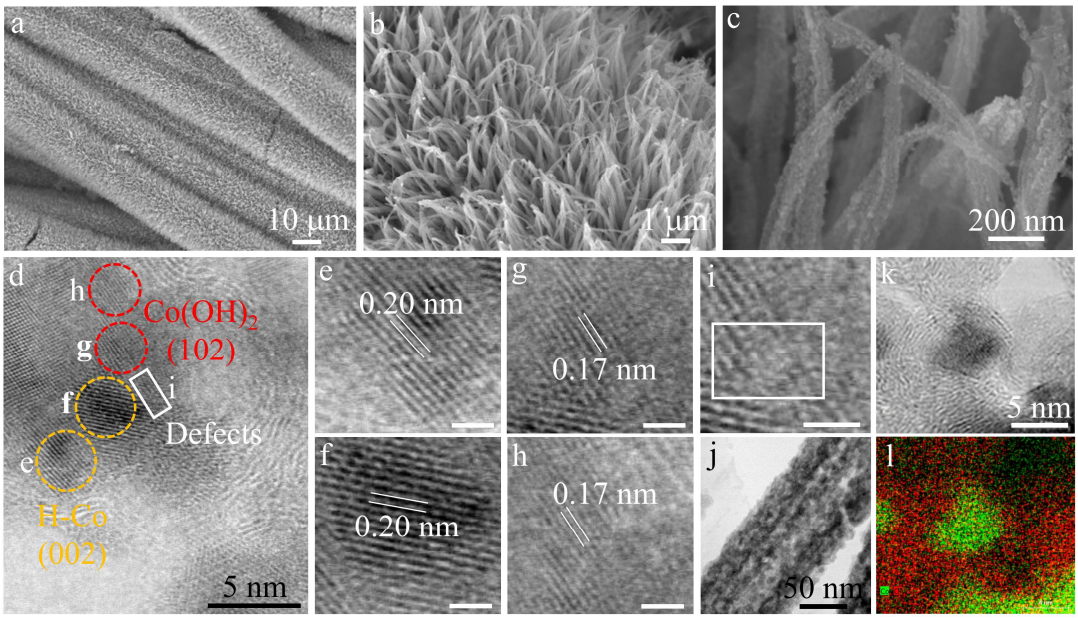

Fig. 4. a–c) SEM images of the evolved H-Co/$Co(OH)_2$/C catalyst at different magnifications. d–i) HRTEM characterization of different crystalline areas in the H-Co/$Co(OH)_2$/C catalyst to reveal the co-existence of H-Co phase, $Co(OH)_2$ phase and the defects sites adjacent to the interphase of H-Co and $Co(OH)_2$. j) Low magnification TEM image of the H-Co/$Co(OH)_2$/C nanowire. k, l) Selected area EDX element mapping results to reveal the core/shell structure (Green color: Co, Red color: Carbon).

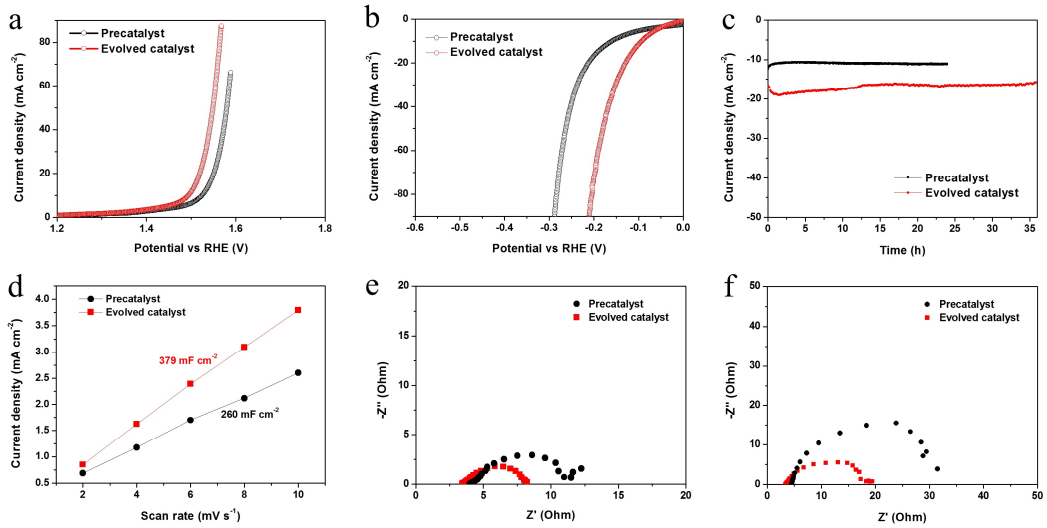

Fig. 5. a) OER and b) HER performance comparison of H-Co/C precatalyst and evolved catalyst H-Co/$Co(OH)_2$/C via LSV measurements. c) Long-term cathodic polarization of H-Co/C precatalyst and evolved H-Co/$Co(OH)_2$/C catalyst at −1.15 V vs Ag/AgCl. d) ECSA comparison of precatalyst and the evolved catalyst. Reduced charge transfer resistance of H-Co/$Co(OH)_2$/C catalyst compared with H-Co/C precatalyst respectively worked for e) OER and f) HER.

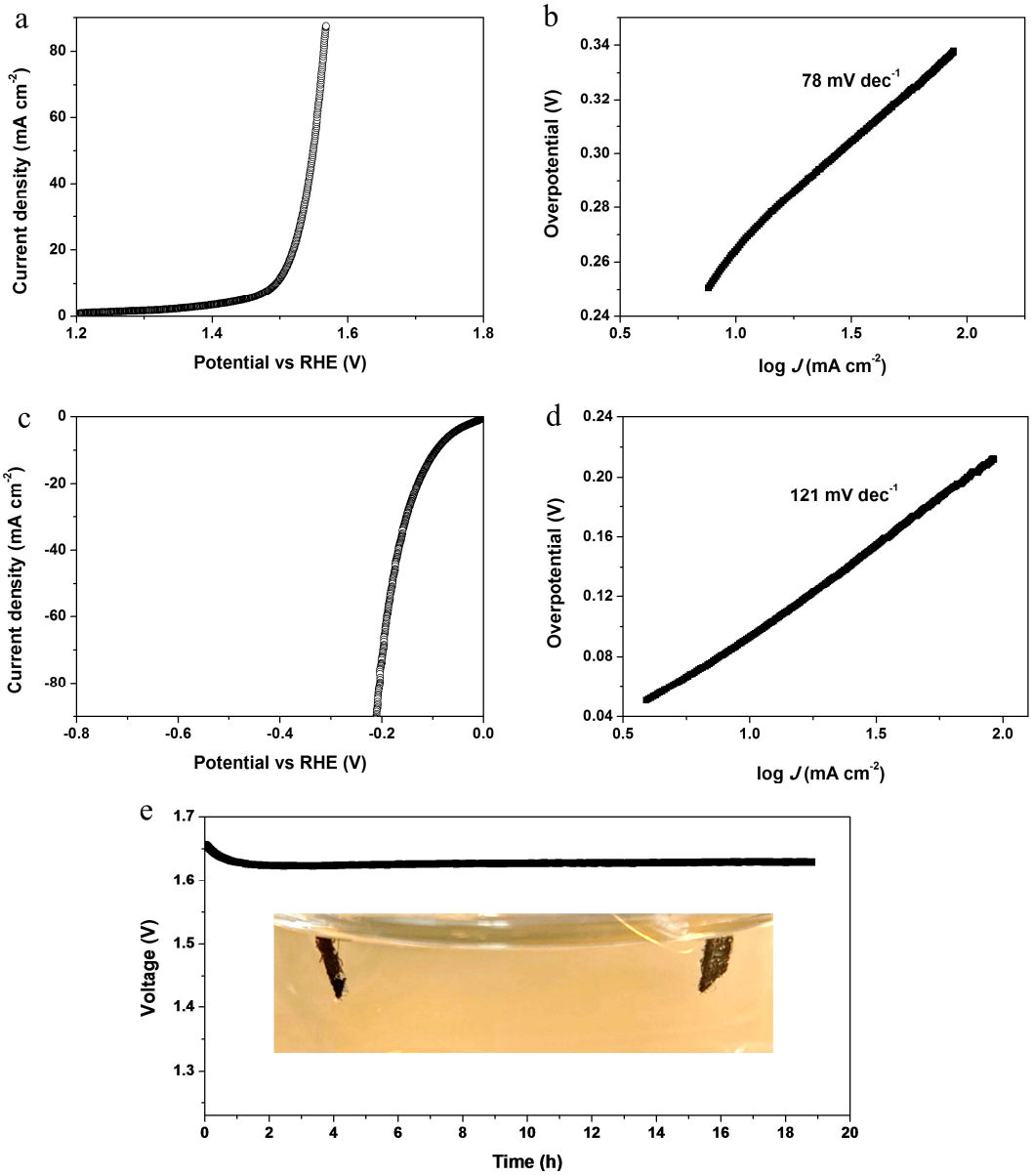

Fig. 6. a,b) OER, and c,d) HER performance of the electrochemically evolved H-Co/$Co(OH)_2$/C electrocatalyst (a and c present the LSV profiles, b and d present the Tafel slopes). e) Full cell performance of electrochemically evolved H-Co/$Co(OH)_2$/C electrocatalyst, with presenting the electrolysis voltage vs time profile when kept at a constant current density of 10 mA cm^{-2}. Inset shows the evolved gas bubbles on both anode and cathode in the electrolyzer.

Table 1

Water splitting performance of H-Co/$Co(OH)_2$/C compared with state-of-the-art electrocatalysts in alkaline water splitting

Catalyst	Current density (10 mA cm^{-2})	HER-η_{10mA} (mV)	Current density (10 mA cm^{-2})	OER-η_{10mA} (mV)	Reference
H-Co/$Co(OH)_2$/C	−10	93	10	264	This study
$Co(OH)_2$/CNT	−10	170	10	270	[34]
Co-CoO_x/C	−10	232	10	260	[38]
Co NP/CNT/G	−10	108	–	–	[41]
Co NP/B, N-C	−10	117	10	302	[42]
Co NP/CNT	−10	190	10	320	[48]
S doped CoO_x	−10	136	100	370	[49]
$Co(OH)_2$/PANI	−10	90	–	–	[50]
Co NP/YRCO	–	–	10	250	[51]

NP, nanoparticle; CNT, carbon nanotube; B, N-C, B/N-co doped carbon; YRCO, yttrium ruthenate pyrochlore oxide; G, graphene; PANI, polyaniline